Colinearity of Photon Path-Density Maxima with Interference Intensity Peaks

by

Brian K. Davis

Research Foundation of Southern California, Inc.
8861 Villa La Jolla Drive, # 13595, CA 92039

(Published April 19, 2017)

Summary. Statistical analysis of reconstructed and Bohmian photon trajectories during self-interference has revealed that path density maxima coincide with intensity peak locations at correlation coefficients exceeding 0.99 and error probability of a 5- to 6-sigma event. The colinearity established between path-density maxima and photon-intensity peaks provides the strongest known quantitative corroboration that the paths obtained resolve the 'which way' problem in the quantum theory of interference.

Key words: *photon interference*; *fringe locations*; *path clusters*; *colinear distributions*; *error estimate*

2. Introduction.

Average photon trajectories reconstructed by Kocsis et al. (2011) and Bohmian photon paths derived by Davidodvic et al. (2013) were recently revealed to exhibit density maxima at locations that correlate with self-interference intensity peaks, at a 4- to 5-sigma risk of error (Davis, 2016, 2017a). This finding quantitatively corroborated the former assessment that the paths obtained resolved the 'which way' problem in the quantum theory of interference – highlighted in the Feynman Lectures as "a phenomenon which is impossible, *absolutely* impossible*,* to explain in any classical way and which has in it the heart of quantum mechanics" (Feynman et al., 1965). It had appeared the uncertainty principle (Heisenberg, 1927) precluded the reconstruction of quantum trajectories, prior to the realization that averaging over weak measurements (Aharonov, Alberts and Vaidman, 1988) of particle momentum furnished a theoretically viable way to reconstruct Bohmian trajectories (Wiseman, 2007).

The present study sought to strengthen the colinear relation established between peaks in path-density and intensity during photon self-interference. Results bearing on fringe formation, intra-fringe clustering by photon paths, and goodness of fit between global distributions of path-density and photon-intensity are presented. An expanded set of density and intensity correlations is also examined. It includes path-dependent and path-independent intensities, with peaks also from far field optics. Weighted average peak locations, based on upper-half values, were utilized in these correlations. Reduced correlation error probabilities, in the 5- to 6-sigma range, resulted.

3. Fringe formation

Solitary photons clustered to form well-defined interference fringes on imaging planes at 3.2 to 7.7 m from a super-cooled InGaAs quantum-dot source, in the 'which-way' experiment of Kocsis et al. (2011). The number of photons in each peak, or trough, within the resulting interferograms were estimated, in this study, from their area (Fig. 1a). Half-gaussian areas in peaks, with usually unequal troughs, were equated to ½ $(\sqrt{2\pi}\, h_i\, \sigma_i)$, where the standard deviation, σ_i (i = 1,2), is $w_i/\sqrt{2 \ln 2}$.

With photon density scaled to interferogram size, the progress of interference could be tracked from changes in the number of photons within fringe dark and light regions.

Figure 1b reveals a linear increase in the relative frequency, f, of peak photons accompanied extensions in flight time (t)/distance (d): $f(t) = 0.031t - 0.239$ ($f(d) = 0.103d - 0.239$) with a coefficient of determination, $r^2 = 0.99$. Conversely, a linear decrease occurred in the relative frequency of non-peak photons (see Appendix, Figure 1b for photon counts). This implies, to a first approximation, that the interference pattern produced by solitary photons arose within a zone bounded by f = 0 and 1: $7.71 \leq f(t) \leq 39.97$ ns, or $2.32 \leq f(d) \leq 12.03$ m.

Peak and non-peak photon counts attributed to interferograms at four imaging planes appear in Fig. 1c. The total number of photons in each increased with distance: 235,736 (3.2 m), 321,191 (4.5 m), 358,340 (5.6 m), and 480,139 (7.7 m). By contrast, the number of non-peak photons remained virtually constant: 214,950 (3.2 m), 252,009 (4.5 m), 234,107 (5.6 m), and 216, 049 (7.7 m). When the depletion of non-peak photons would have been anticipated, additions to intensity peaks almost solely accounted for the increase: 21,641 (3.2 m), 69,182 (4.5 m), 124,233 (5.6 m), and 264,030 (7.7 m). With a constant photon flux of 1 photon per 484 μs (Fig. 1b) and constant 15 s exposure intervals, producing around 31,000 solitary photons, progressively more exposures with distance might account for the apparent photon amplification in the interferometer. Photon amplification may also accompany the weak value determination of photon momentum (Aharanov et al., 1988; Hallaji, 2016).

Figure 1. Fringe formation from photon self-interference. (a) T_1, T_2 mark regions (stippled) of trough photons. Peak regions P_1, P_2, were half-gaussian areas, possibly unequal, with respective heights, h_1 and h_2, and widths, at half-maximum height, of w_1 and w_2. (b) The global frequency of peak photons, f, increased linearly (r^2, coefficient of determination) during flight up to 25.7 ns (7.7 m), at an estimated flux of one photon per 484 μs. (c) A largely constant number of non-peak photons occurred in interferograms at 3.2, 4.5, 5.6, and 7.7 m. Peak photons (unshaded area) increased linearly, resulting in the total number of photons per interferogram (upper line) increasing at a broadly constant rate with distance. Dashed lines represent extrapolations to an initial, pre-photon emission state This figure is based on experimental observations reported by Kocsis et al. (2011).

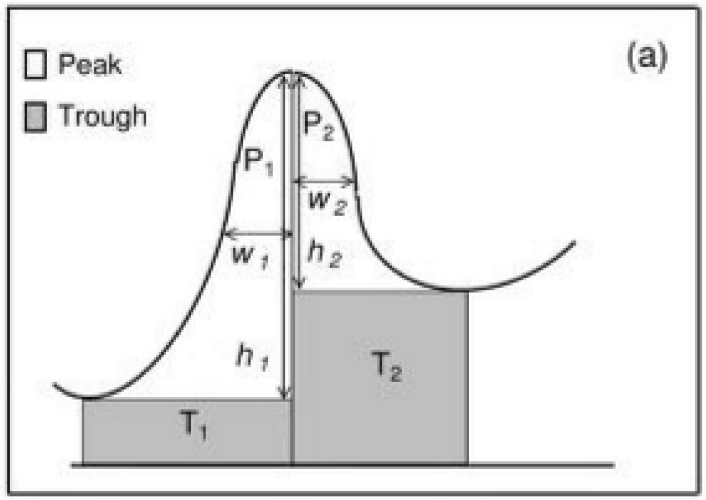
Peak
Trough
(a)
P1
P2
w1
w2
h1
h2
T1
T2

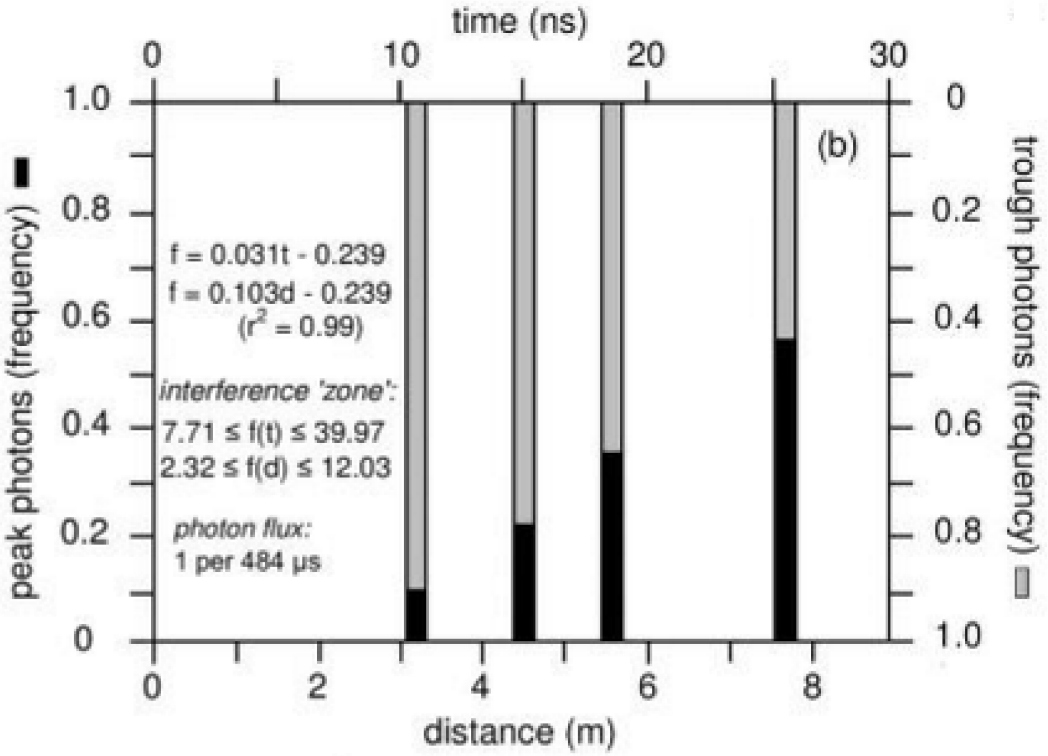
time (ns)
0
10
20
30
(b)
peak photons (frequency)
trough photons (frequency)
f = 0.031t - 0.239
f = 0.103d - 0.239
(r2 = 0.99)
interference 'zone':
7.71 ≤ f(t) ≤ 39.97
2.32 ≤ f(d) ≤ 12.03
photon flux:
1 per 484 µs
distance (m)

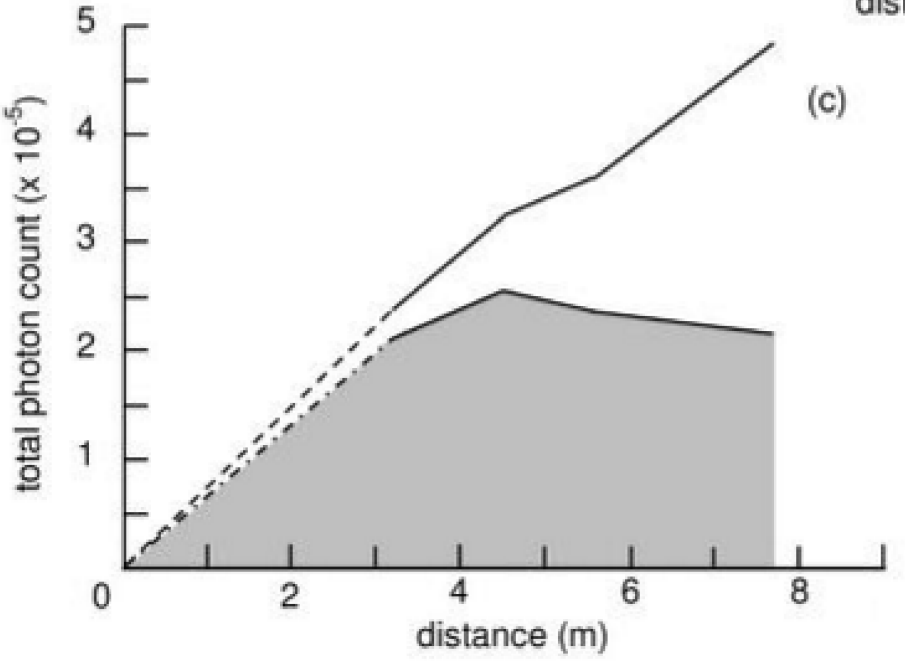
(c)
total photon count (x 10-5)
distance (m)

The high, nearly constant background of diffuse, non-peak photons in Fig. 1c understates its actual magnitude, since a constant background, about half the reported data (Coffey and Wyatt, 2011), was deducted from the interferograms obtained by Kocsis et al. (2011). It may be noted, in this connection, that all previous attempts to identify the photon flight-path in interference relied on strong measurements, which suppressed of interference, producing instead a simple single-slit photon distribution (Bohr, 1949; Feynman et al., 1965).

In the present context, the number of diffuse background photons is not considered relevant. The objective in this endeavor being to find, and quantitate, a feature of the reconstructed and Bohmian photon trajectories that demonstrates the occurrence of interference. This shall take the form of establishing that peak locations in path-density are colinear with those of photon intensity.

Since the interferogram at 7.7 m contained the highest number of peak photons, it has served as the source of peak locations. The remaining sections of this report, consequently, focus on this distance. According to the empirical relation in (Fig. 1b), interference beyond 7.7 m could achieve an even higher peak photon frequency. Thus, correlations with a lower error probability than that obtained, conceivably,can be found in interferograms beyond 7.7 m.

4. Path density and photon intensity distributions

The bottom panel in Fig. 2 depicts the spectrum of 80 reconstructed photon paths (Kocsis et al., 2011) on the axis (x-axis) transverse to the direction of flight (z-axis), at distances measured from the optical center. Consistent with interference, they form a broadly symmetric distribution of clusters around a prominent central cluster. The next panel shows these clusters form a somewhat ragged, but distinct pattern of path-density peaks; where path-density is specified as the reciprocal distance between adjacent (left to right) paths - an average density being assigned to merged paths. On marking path positions within the interferogram (third panel[1]), it becomes apparent that most paths are clustered within the upper-half of interference fringe peaks.

[1]Peak +3 is missing; it is present in the path-density distribution (second panel, at path 78) and interferogram of oppositely polarized photons (not shown).

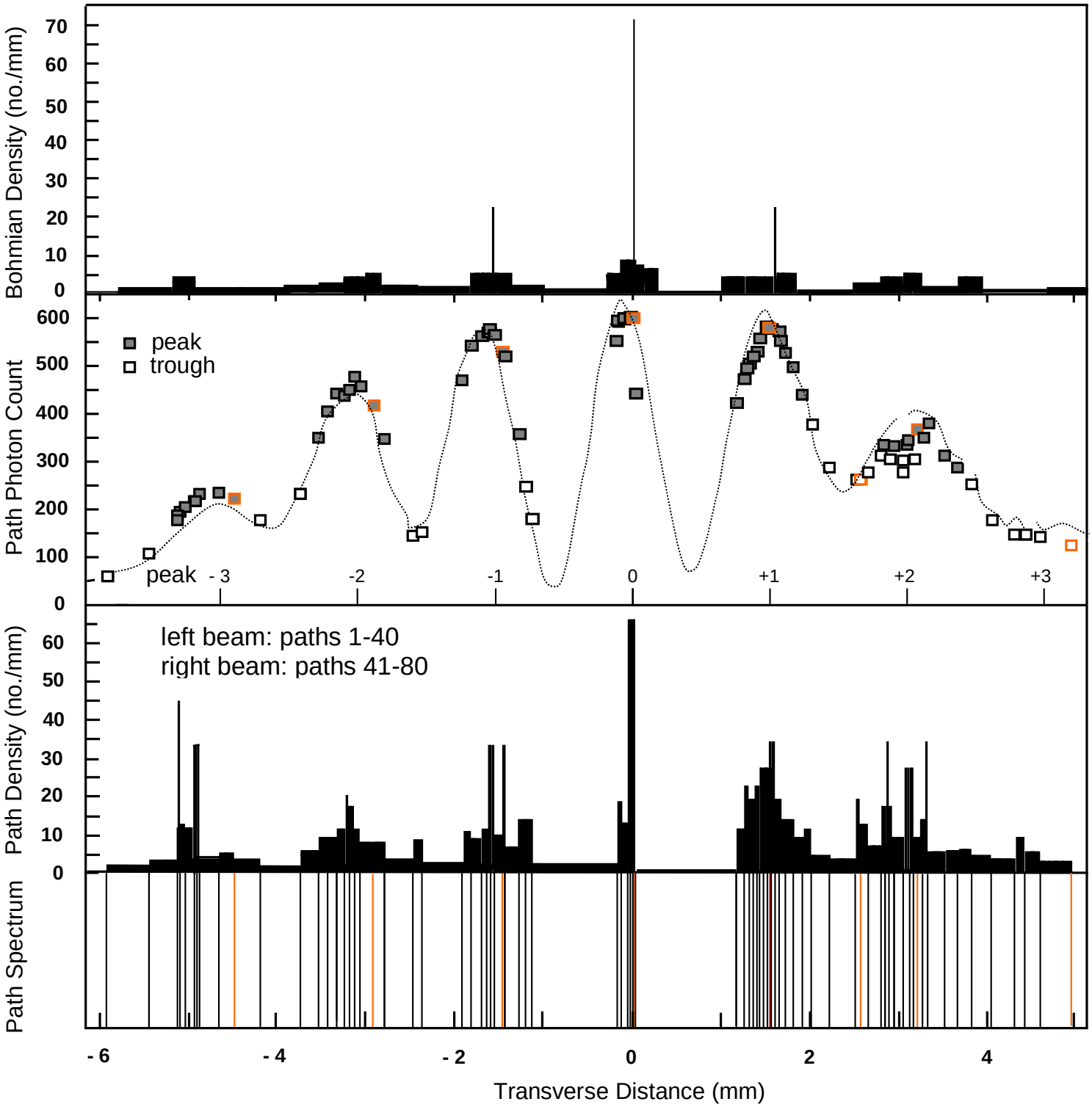
Bohmian Density (no./mm)
70
60
50
40
30
20
10
0
Path Photon Count
600
500
400
300
200
100
0
peak
trough
peak
- 3
-2
-1
0
+1
+2
+3
Path Density (no./mm)
60
50
40
30
20
10
0
left beam: paths 1-40
right beam: paths 41-80
Path Spectrum
- 6
- 4
- 2
0
2
4
Transverse Distance (mm)

Figure 2. Correspondence between photon path-density and intensity distributions produced by self-interference. *Path Spectrum* shows the transverse distance of 80 photon paths, reconstructed by Kocsis et al. (2011), measured from the optical center of the 7.7 m interferogram. An orange vertical line identifies each tenth path. Left- and right-side paths are from the same-side photon beam. *Path Density* portrays the distribution of photon path-density, representing the reciprocal distance between adjacent (left-to-right) trajectories. Path clusters can be seen to occur equidistant from a dense central cluster, indicative of interference. *Path Photon Count* depicts light intensity in the interference pattern, together with the location of each path. The paths conspicuously cluster within fringe peaks (upper-half) of an aggregate distribution of clockwise and counter-clockwise polarized photons (traced dotted line indicates peak locations). *Bohm Density* portrays the density profile of thirty-six photon trajectories derived on applying Bohmian mechanics to the Kocsis et al. interferometer (Davidovic et al., 2013).

Table 1 shows that reconstructed photon paths cluster to a highly significant degree within peaks of photon intensity on self-interference. Among the smaller number of Bohmian paths, the fraction located within fringe peaks closely approached statistical significance. Combining these probabilities reveals significant path clustering existed within photon self-interference peaks.

Table 1. Extent of clustering by reconstructed and Bohmian photon paths into interference peaks at 7.7 m from source[a]

Paths	Peak (no. paths)	Trough (no. paths)	p [b]
Reconstructed[c]	61	19	**5.29E-6**
Bohmian[d]	23	13	0.062
Total	84	32	**4.85E-3**

[a] **Drawn from results in Fig. 2.**

[b] ***p*, probability of path clusters within fringe peaks (upper-half), based on a compressed boostrap calculation (Davis, 2017b). Bold, statistically significant peak clusters. Probabilities from each source were combined by the method of Fisher (1925).**

[c] **Photon paths are from Kocsis et al. (2011) and [d]Davidovic et al. (2013).**

Table 2 shows no significant difference in the goodness of fit between complete distributions of photon counts, from the 7.7 m interferogram, and path-density among reconstructed photon trajectories (Kocsis et al., 2011). Bohmian photon trajectories deduced by Davidovic et al. (2013) for the interferometer assembled by Kocsis and coworkers, likewise, displayed no significant difference with the observed distribution of photon intensities or their experimentally determined paths.

Table 2. Goodness of fit by reconstructed path-density versus photon intensity and Bohmian path-density distributions at 7.7 m[a]

Distributions	N	D_{max}	p [b]
Recon. paths *v*. Photon counts[c]	79, 80	0.073	0.653
Recon. paths *v*. Bohmian paths	79, 35	0.194	0.162
Total			0.343

[a] **Drawn from results in Fig. 2. See Appendix for distributions.**

[b] ***p*, probability of distributions being the same, based on Kolmogorov-Smirnov tests and Goodman (1959) X^2 approximation. No significant difference is apparent, validating the null hypothesis. Probabilities from each comparison were combined by the method of Fisher (1925).**

[c] **The source of each type of path appears under Table 1.**

5. Correlations between sets of path-density and photon-intensity peak locations

Figure 3 shows correlations between sets of peak locations for path-density and photon intensity, in Fig. 2 distributions. Also included are path-independent peak locations obtained on averaging over

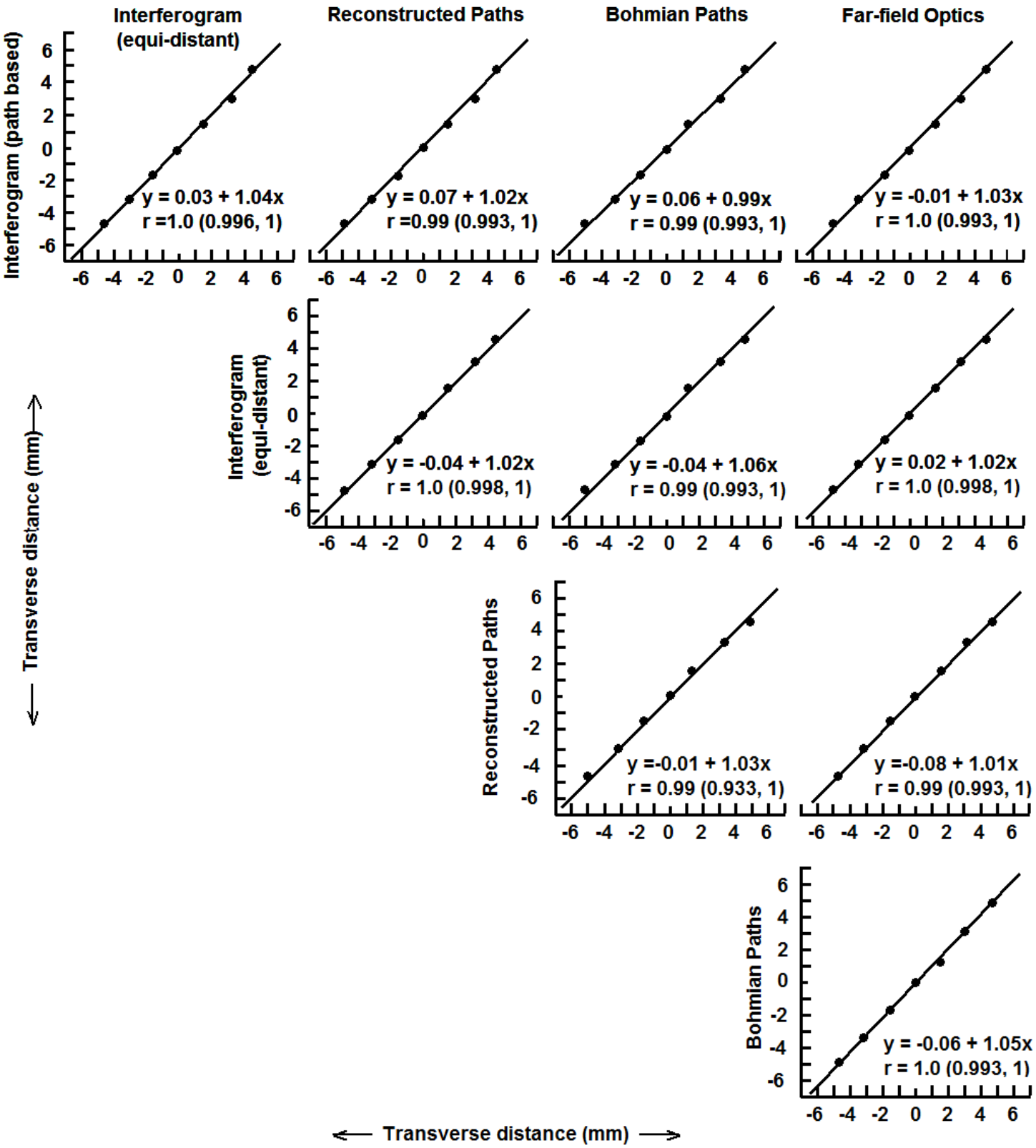
Interferogram (equi-distant)
Reconstructed Paths
Bohmian Paths
Far-field Optics
Interferogram (path based)
y = 0.03 + 1.04x
r =1.0 (0.996, 1)
y = 0.07 + 1.02x
r =0.99 (0.993, 1)
y = 0.06 + 0.99x
r = 0.99 (0.993, 1)
y = -0.01 + 1.03x
r = 1.0 (0.993, 1)
Interferogram (equi-distant)
y = -0.04 + 1.02x
r = 1.0 (0.998, 1)
y = -0.04 + 1.06x
r = 0.99 (0.993, 1)
y = 0.02 + 1.02x
r = 1.0 (0.998, 1)
Reconstructed Paths
y =-0.01 + 1.03x
r = 0.99 (0.933, 1)
y =-0.08 + 1.01x
r = 0.99 (0.993, 1)
Bohmian Paths
y = -0.06 + 1.05x
r = 1.0 (0.993, 1)
Transverse distance (mm)
Transverse distance (mm)

Figure 3. Correlations between sets of peak locations among observed and predicted photon intensity, and reconstructed- and Bohmian-path density. Each matched pair exhibits a strong transverse distance correlation. Pearson correlation coefficients, r, exceed 0.99 in all pairs, at a distance of 7.7 m from the photon source within a split-beam interferometer. In parenthesis are 95 per cent confidence intervals on each correlation coefficient. A set of linear regression equations result that effectively reduce to y ≈ x correspondences.

equi-spaced and far field optics intensities. These correlations therefore span experimental (Kocsis et al., 2011) and theoretical (Davidovic et al., 2013, Morin, 2010) photon interference intensity and path density distributions. Far field optics intensity (Fraunhofer region) being specified as,

$$I_x/I_o = (D/\sqrt{x^2 + D^2})(\cos^2(x\pi d/(\lambda\sqrt{x^2 + D^2}))),$$

where I_x and I_o refer to intensity at the distance x and optical center, respectively: $-5 \leq x \leq 5$, distance from optical center. With all lengths in mm, image plane distance, D = 7700; inter-beam distance at source, d = 4.69; wavelength, λ = 943E-6. Indicative of a highly significant goodness of fit between each set of peak locations, all correlation coefficients exceed 0.99. The array of linear regression equations obtained thus reduces to ten, y ≈ x relations.

Peak locations in the path-based interferogram were weighted average of intensities at x-axis locations of reconstructed photon trajectories, from within a peak upper-half. Each intensity was weighted by its contribution to the global intensity distribution and normalized with respect to the set of peak intensities: $\overline{X}_i = \sum_j X_{ij}w_{ij}$, where $\overline{X}_i$ is the designated location of peak-i on the x-axis, X_{ij} refers to the location of the j^{th} photon path, in the peak-i upper-half, with w_{ij} a normalized photon intensity weighting factor ($\sum_j w_{ij} = 1$). A second, path-independent interferogram intensity distribution was constructed (Fig. 3), to eliminate the possibility of a path-based bias. Intensities at each of eighty equi-distant x-axis locations, on the $-5 \leq x \leq 5$ mm interval, then determined peak locations.

Table 3 lists statistical parameters characterizing the set of peak location correlations in Fig. 3. Among them are two-tail probabilities for validity of the null hypothesis, stipulating that peak locations

in each pair are from different distributions. They demonstrate this outcome to be extremely unlikely, being equivalent to occurrence of a 5- to 6-sigma event, for each correlation.

Table 3. Error probability parameters for correlations in the location of peaks in photon path-density and intensity in Figure 3.[a]

Source of Peaks	r^2	t_5	*p*	σ
Interferogram: path				
v. Equi-distant	0.997	61.53	2.146E-8	5.5 - 6.0
v. Recon. paths	0.997	42.92	1.296E-7	5.0 - 5.5
v. Bohmian paths	0.998	51.04	5.459E-8	5.0 - 5.5
v. Far-field optics	0.999	82.24	5.038E-9	5.5 - 6.0
Interferogram: equi-distant				
v. Recon. paths	0.999	82.29	5.022E-9	5.5 - 6.0
v. Bohmian paths	0.999	47.69	7.658E-8	5.0 - 5.5
v. Far-field optics	0.999	112.52	1.051E-9	> 6.0
Recon. paths				
v. Bohmian paths	0.998	54.11	4.078E-8	~ 5.5
v.Far-field optics	0.999	64.03	1.759E-8	5.5 - 6.0
Bohmian paths				
v. Far-field optics	0.998	51.58	5.189E-8	5.0 - 5.5

[a] **Parameters: r^2, coefficient of determination; t_5, t-value of correlation at 5 degrees of freedom; *p*, t-distribution probability; σ, range in number of standard deviations to contain *p*.**

6. Concluding Remarks

The location of path-density maxima at a 7.7 m imaging plane, in a split-beam interferometer (Kocsis et al., 2011), were shown to correlate with photon-intensity peaks at an error probability reduced to 5-

to 6- sigma (Table 3). This provides compelling statistical evidence crediting the photon trajectories, reconstructed by averaging over weak transverse momentum measurements (Kocsis et al., 2011) and by extending Bohmian mechanics to this massless particle (Davidovic et al., 2013), with resolving the 'which way' issue in the quantum theory of interference (Bohr, 1949; Feynman et al., 1965). Increased precision in determining average peak locations, achieved in this study, is attributed to restricting the weighting factors to upper-half path-density and photon-intensity values. Further optimization of colinearity between photon path-density maxima and intensity peaks, at a specified stage of interference, through additional restrictions on peak values would require any gain in location precision to outweigh likely increases in variability from reliance on a smaller sample size.

When combining the observed strength of colinearity between path-density maxima and photon-intensity peaks (Table 3) with the direct 'which way' pattern formed by reconstructed and Bohmian paths (Kocsis et al., 2001; Davidovic et al., 2013), photons within each self-interference fringe can be deduced to have travelled by a single trajectory from the nearest slit/beam. Given that phase differences responsible for interference derive from flight paths of different length, exclusion of simultaneous passage on an alternative track might appear to imply photon non-locality during self-interference. The DeBroglie-Bohm interpretation of quantum mechanics (DeBroglie 1923, 1970; Bohm 1952a,b), however, explicitly embodies coexistence of a solitary particle and its accompanying field. Flow lines from the transverse photon electromagnetic field waves were inferred by Davidovic et al. (2013) to alter the photon trajectory in self-interference. They directly linked the magnitude of photon transverse momentum, within the interferometer of Kocsis and coworkers, to the magnitude of its accompanying Poynting vector (real part).

References

Aharanov Y, Albert DZ, Vaidman L 1988. How the result of a measurement of a component of the spin of a spin-½ particle can turn out to be 100. *Phys. Rev. Lett*. **60**, 1351-1354. http://dx.doi.org/10.1103/PhysRevLett.60.1351

Bohm D 1952a. A suggested interpretation of the quantum theory in terms of 'hidden variables' I

Phys. Rev. **85**, 166-198. https://doi.org/10.1103/physrev.85.166

Bohm D 1952b. A suggested interpretation of the quantum theory in terms of 'hidden variables' II *Phys. Rev.* **85**, 180-193. https://doi.org/10.1103/physrev.85.183

Bohr N 1949. Discussion with Einstein on Epistemological Problems in Atomic Physics. In: *Albert Einstein: Philosopher-Scientist* Ed. PA Schlipp. Evanston: The Library of Living Philosophers. 1949. Reprinted in: *Quantum Theory and Measurement* Eds. JA Wheeler, WH Zurek Princeton: Princeton Univ. Press pp. 9-49, 1983

Coffey TM, Wyatt RE 2011. Comment on "Observing the average trajectories of single photons in a two-slit interferometer" arXiv:1109 4436v1

Davidovic M, Sanz AS, Arsenovic D, Bozic M, Miret-Artes S 2009. Electromagnetic energy flow lines as possible paths of photons. *Phys. Scr.* **T**135/014009 http://dx.doi.org/10.1088/0031-8949/2009/T135/014009

Davidovic M, Sanz AS, Bozic M, Arsenovic D, Dimic D 2013. Trajectory-based interpretation of Young's experiment the Arago-Fresnel laws and the Poisson-Arago spot for photons and massive particles. *Phys. Scr.* **T**153/014015 http://dx.doi.org/10.1088/0031-8949/2013/T153/014015

Davis BK 2016. Photon path density strongly correlates with photon intensity in self-interference. http://archive.org/details/PhotonPathDensity

Davis BK 2017a. Photon path density strongly correlates with photon intensity in self-interference: Inclusions. http://archive.org/details/PhotonPathDensityInclusions4i17

Davis BK 2017b. The compressed bootstrap. http://archive.org/details/CompressedBootstrap

De Broglie L 1923. Waves and quanta. *Nature* **112**, 540. https://doi.org/10.1038/112540a0

De Broglie L 1970..The reinterpretation of wave mechanics. *Foundations of Physics* **1**, 5-15.

Feynman RP, Leighton RB, Sands M 1965. *The Feynman Lectures on Physics: Quantum Mechanics* Reading: Addison-Wesley.

Fisher RA 1925. *Statistical Methods for Research Workers*. Edinburgh: Oliver & Boyd

Goodman LA (1959) Simple statistical methods for scalagram analysis. *Psychometrika* **24**, 29-43. http://dx.doi.org/10.1007/BF02289761

Hallaji M (2016) *Weak value amplification of a post-selected photon.* Thesis, Univ. Toronto http://www.tspace.library.utoronto.ca/bitstream/1807/73013/1/Hallaji_Matin_201606_PhD_thesis.pdf

Heisenberg W 1927. Über den anschaulichen inhalt der quantentheoretischen kinematik and mechanik. *Z. Physik* **43**, 172-198. English translation: *Quantum Theory and Measurement* Eds. JA Wheeler, WH Zurek Princeton: Princeton Univ. Press pp. 62-84, 1983.

Kocsis S, Braverman B, Ravets S, Stevens MJ, Mirin RP, Shalm LK, Steinberg AM 2011. Observing the average trajectories of single photons in a two-slit interferometer. *Science* **332**, 1170-1173. http://dx.doi.org/10.1126/science.1202218

Mandel L 1999. Quantum effects of one-photon and two-photon interference. *Rev. Mod. Phys.* **71**, S274-S282 http://dx.doi.org/10.1088/1367-2630/9/6/165

Morin DJ 2010. Interference and Diffraction. http://people.fas.harvard.edu/~djmorin/waves/interference.pdf/

Wiseman HM 2007 Grounding Bohmian mechanics in weak values and bayesianism. *New J. Phys*. **9**, 165, pp. 1-13 http://dx.doi.org/10.1088/1367-2630/9/6/165

Appendix

Photon counts obtained for peak and trough areas at indicated interference fringes in **Figure 1(b**), together with times/distances of flight.

time (ns)	distance(m)	site	photon count										
			fringe : -4	-3	-2	-1	-0	+0	+1	+2	+3	+4	total
10.67	3.2	peak	1345	13580	1793	1697	1219	1025	645	337	0	0	21641
		trough	←		98234	→	←			115861	→		214095
													235736
15.01	4.5	peak	961	1922	13772	12485	6726	4036	16305	12600	375	0	69182
		trough	14267	64515	15668	7148	721	4804	23763	47500	73623	→	252009
													321191
18.68	5.6	peak	0	7042	22925	23089	15219	9687	24211	19310	2750	0	124233
		trough	2525	37370	34424	14227	2314	5470	30559	53964	53254	→	234107
													358340
25.68	7.7	peak	0	14066	38422	59484	38622	28368	51299	31465	2364	0	264090
		trough	←	30138	32796	17285	3989	9640	41031	65900	15270	→	216049
													480139

t (ns)	d (m)	peak (freq.)
10.67	3.2	0.0918
15.01	4.5	0.2154
18.68	5.6	0.3467
25.68	7.7	0.5500

Cumulative distributions of normalized photon path-density and intensity, at specified positions determined from interference patterns in Fig. 2, used in **Table 1** to assess clustering.[a]

Bohm paths		Recon. paths		Diff.
x-axis (mm)	density: cumul. distribn.	x-axis (mm)	density: cumul. distribn.	
-7.30	0.0029		0	0.00289
	0.0029	-6	0.002	0.00138
	0.0029	-5.92	0.0038	0.0009
-5.75	0.0105		0.0038	0.00668
	0.0105	-5.44	0.0365	0.02601
-5.16	0.0281		0.0365	0.00834
	0.0281	-5.12	0.0454	0.01725
	0.0281	-5.10	0.0536	0.02542
	0.0281	-5.02	0.0781	0.04993
	0.0281	-4.93	0.1026	0.07445
-4.91	0.0326		0.1026	0.07003
	0.0326	-4.90	0.1060	0.07341
	0.0326	-4.87	0.1100	0.0775
	0.0326	**-4.65**	0.1125	0.07995
	0.0326	-4.48	0.1141	0.08158
	0.0326	-4.18	0.1178	0.08521
-3.90	0.0439		0.1178	0.07385
	0.0439	-3.74	0.1248	0.08086
	0.0439	-3.54	0.1318	0.08786
-3.51	0.0606		0.1318	0.07112
	0.0606	-3.43	0.1399	0.07929
	0.0606	-3.33	0.1539	0.0933
-3.24	0.0805	-3.24	0.1662	0.08568
	0.0805	-3.19	0.1744	0.09385
	0.0805	**-3.13**	0.1825	0.10202
	0.0805	-3.04	0.1872	0.10669
-3.02	0.1017		0.1872	0.08548
	0.1017	-2.91	0.1896	0.08782
-2.81	0.1131		0.1896	0.07646
	0.1131	-2.80	0.1957	0.08259
	0.1131	-2.48	0.1973	0.0842
-2.41	0.1210		0.1973	0.07624
	0.1210	-2.37	0.2048	0.08379
	0.1210	-1.92	0.2110	0.08991
-1.85	0.1398		0.2110	0.07121
	0.1398	-1.82	0.2191	0.07938
	0.1398	-1.70	0.2436	0.10389
-1.61	0.2458	**-1.61**	0.2682	0.02238
	0.2458	-1.58	0.2752	0.02939
-1.57	0.2645		0.2752	0.01068
	0.2645	-1.55	0.2997	0.03519
	0.2645	-1.45	0.3041	0.03965
	0.2645	-1.42	0.3139	0.04945

	Recon. paths	Photon count	Diff.
x-axis (mm)	density: cumul. distribn.	intensity: cumul. distribn.	
-6	0.002	0.0020	0.001966
-5.92	0.0038	0.0058	0.001815
-5.44	0.0365	0.0114	0.025068
-5.12	0.0454	0.0177	0.027689
-5.10	0.0536	0.0243	0.029273
-5.02	0.0781	0.0315	0.046608
-4.93	0.1026	0.0390	0.063551
-4.90	0.1060	0.0467	0.059263
-4.87	0.1100	0.0546	0.055484
-4.65	0.1125	0.0619	0.050561
-4.48	0.1141	0.0678	0.046297
-4.18	0.1178	0.0757	0.042063
-3.74	0.1248	0.0873	0.037466
-3.54	0.1318	0.1006	0.031197
-3.43	0.1399	0.1152	0.024719
-3.33	0.1539	0.1302	0.023783
-3.24	0.1662	0.1455	0.020702
-3.19	0.1744	0.1612	0.013143
-3.13	0.1825	0.1764	0.006173
-3.04	0.1872	0.1901	0.002921
-2.91	0.1896	0.2016	0.01209
-2.80	0.1957	0.2066	0.010877
-2.48	0.1973	0.2116	0.014284
-2.37	0.2048	0.2273	0.022472
-1.92	0.2110	0.2454	0.034433
-1.82	0.2191	0.2642	0.04504
-1.70	0.2436	0.2833	0.039699
-1.61	0.2682	0.3024	0.03422
-1.58	0.2752	0.3213	0.046191
-1.55	0.2997	0.3389	0.039276
-1.45	0.3041	0.3562	0.052123
-1.42	0.3139	0.3681	0.054213
-1.26	0.3237	0.3765	0.052765
-1.18	0.3245	0.3824	0.057898
-1.11	0.3385	0.4009	0.062374
-0.16	0.3474	0.4206	**0.073221**
-0.11	0.3964	0.4406	0.044154
-0.03	0.4455	0.4607	0.015185
-0.01	0.4945	0.4808	0.013686

Table 1. distributions (cont.)

-0.98	0.2841		0.3385	0.05439
-0.34	0.3040		0.3385	0.03452
	0.3040	-0.16	0.3474	0.04343
-0.11	0.3437	-0.11	0.3964	0.0527
	0.3437	-0.03	0.4455	0.10172
	0.3437	-0.01	0.4945	0.15075
0.00	0.6618	**0.00**	0.5435	0.11828
0.01	0.6971	0.01	0.5441	0.15299
	0.6971	0.03	0.5523	0.14482
0.14	0.7236		0.5523	0.17132
0.31	0.7300		0.5523	0.17768
1.01	0.7459		0.5523	**0.19359**
	0.7459	1.18	0.5687	0.17724
	0.7459	1.27	0.5827	0.16324
1.29	0.7618		0.5827	0.17914
	0.7618	1.32	0.5990	0.1628
	0.7618	1.37	0.6186	0.14319
	0.7618	1.41	0.6382	0.12358
	0.7618	1.45	0.6578	0.10397
	0.7618	1.49	0.6824	0.07946
	0.7618	1.52	0.7069	0.05494
	0.7618	**1.55**	0.7314	0.03043
1.57	0.8678		0.7314	0.13645
	0.8678	1.58	0.7454	0.12244
1.61	0.8865	1.61	0.7552	0.13135
	0.8865	1.67	0.7650	0.12154
	0.8865	1.74	0.7715	0.115
	0.8865	1.81	0.7797	0.10683
1.85	0.8939		0.7797	0.11423
	0.8939	1.92	0.7830	0.11096
	0.8939	2.01	0.7854	0.10851
	0.8939	2.23	0.7994	0.0945
2.46	0.9067		0.7994	0.10723
	0.9067	2.53	0.8083	0.09831
	0.9067	2.58	0.8132	0.09341
	0.9067	2.66	0.8255	0.08115
2.81	0.9254	2.81	0.8500	0.07535
	0.9254	2.87	0.8623	0.06309
	0.9254	2.90	0.8688	0.05656
	0.9254	2.96	0.8884	0.03695
3.05	0.9452		0.8884	0.05683
	0.9452	3.07	0.9080	0.03722
	0.9452	**3.11**	0.9276	0.01761
	0.9452	3.15	0.9342	0.01107
	0.9452	3.18	0.9440	0.00126
	0.9452	3.22	0.9685	0.02325
3.27	0.9570		0.9685	0.01147
	0.9570	3.29	0.9726	0.01555
	0.9570	3.34	0.9768	0.01982

0.00	0.5435	0.5008	0.042753
0.0148	0.5441	0.5155	0.028634
0.0296	0.5523	0.5295	0.022845
1.18	0.5687	0.5451	0.023554
1.27	0.5827	0.5614	0.021242
1.32	0.5990	0.5781	0.02087
1.37	0.6186	0.5954	0.023177
1.41	0.6382	0.6129	0.025287
1.45	0.6578	0.6314	0.026414
1.49	0.6824	0.6506	0.031755
1.52	0.7069	0.6698	0.037097
1.55	0.7314	0.6889	0.042438
1.58	0.7454	0.7080	0.037372
1.61	0.7552	0.7264	0.028793
1.67	0.7650	0.7440	0.021
1.74	0.7715	0.7604	0.011118
1.81	0.7797	0.7750	0.004738
1.92	0.7830	0.7875	0.004577
2.01	0.7854	0.7972	0.011761
2.23	0.7994	0.8058	0.006405
2.53	0.8083	0.8145	0.006143
2.58	0.8132	0.8235	0.010286
2.66	0.8255	0.8339	0.008352
2.81	0.8500	0.8449	0.005149
2.87	0.8623	0.8549	0.007377
2.90	0.8688	0.8661	0.002706
2.96	0.8884	0.8775	0.010912
3.07	0.9080	0.8892	0.018822
3.11	0.9276	0.8992	0.028404
3.15	0.9342	0.9103	0.023832
3.18	0.9440	0.9225	0.021446
3.22	0.9685	0.9341	0.034357
3.29	0.9726	0.9468	0.02576
3.34	0.9768	0.9572	0.019602
3.52	0.9813	0.9667	0.014621
3.69	0.9846	0.9750	0.009533
3.85	0.9874	0.9811	0.006239
4.07	0.9939	0.9860	0.00786
4.33	0.9978	0.9910	0.006866
4.44	1.0000	0.9957	0.004326
4.63		1.0000	

	N = 80-1	**N = 80**
		D_{max} = **0.073221**
Chi sq (df=2) = 0.852		***p* = 0.653**

Table 1. distributions (cont.)

	0.9570	3.34	0.9768	0.01982
	0.9570	3.52	0.9813	0.02427
3.65	0.9570		0.9813	0.02427
	0.9570	3.69	0.9846	0.02754
	0.9570	3.85	0.9874	0.03034
3.93	0.9781		0.9874	0.00923
	0.9781	4.07	0.9939	0.01576
	0.9781	4.33	0.9978	0.01969
	0.9781	4.44	1.0000	0.02186
	0.9781	**4.63**	1.0000	0.02186
4.79	0.9891		1.0000	0.0109
	0.9891		1.0000	0.0109
5.19	0.9959		1.0000	0.00413
5.85	1.0000		1.0000	0
6.93				
N = 36-1		**N = 80-1**	**D_{max} =**	**0.19359**

Chi sq (df=2) = 3.835 ***p*** **= 0.162**

[a] Highlighted values mark location of far field intensity maxima.

Cumul. Distribn., cumulative distribution; Diff., difference.

Photon path-density and corresponding intensity for each reconstructed, or Bohmian, trajectory are listed, together with their transverse position in the interference patterns in **Fig. 2**. Each path is numbered, while those clustered within a peak upper-half are enclosed.

Reconstructed Paths

path no.	x-axis (mm)	path density (no. paths/mm)	photon count
1	-5.92	2.08	59
2	-5.44	3.14	109
3	-5.12	45.05	174
4	-5.10	12.29	188
5	-5.02	11.26	197
6	-4.93	33.78	215
7	-4.90	33.78	226
8	-4.87	4.66	229
9	-4.65	5.63	235
10	-4.48	3.38	221
11	-4.18	2.25	176
12	-3.74	5.01	235
13	-3.54	9.65	347
14	-3.43	9.65	397
15	-3.33	11.26	438
16	-3.24	19.31	447
17	-3.19	16.89	459
18	**-3.13**	11.26	471
19	-3.04	7.69	453
20	-2.91	7.69	412
21	-2.80	3.22	344
22	-2.48	8.45	147
23	-2.37	2.22	150
24	-1.92	10.40	471
25	-1.82	8.45	541
26	-1.70	11.26	562
27	-1.61	33.78	574
28	-1.58	33.78	569
29	-1.55	9.65	568
30	-1.45	33.78	526
31	-1.42	6.14	518
32	-1.26	13.51	356
33	-1.18	13.51	250
34	-1.11	1.06	176
35	-0.16	19.31	553
36	-0.11	12.29	591
37	-0.03	67.57	597
38	-0.01	67.57	600
40	**0.00**	67.57	603

Bohmian Paths

path no.	x-axis (mm)	path density (no. paths/mm)
1	-7.30	0.65
2	-5.75	1.70
3	-5.16	3.96
4	-4.91	0.99
5	-3.90	2.54
6	-3.51	3.75
7	-3.24	4.45
8	-3.02	4.75
9	-2.81	2.54
10	-2.41	1.78
11	-1.85	4.19
12	-1.61	23.75
13	-1.57	4.19
14	-1.33	2.85
15	-0.98	1.55
16	-0.34	4.45
17	-0.11	8.91
18	**0.00**	71.25
19	0.01	7.92
20	0.14	5.94
21	0.31	1.43
22	1.01	3.56
23	1.29	3.56
24	1.57	23.75
25	1.61	4.19
26	1.85	1.66
27	2.46	2.85
28	2.81	4.19
29	3.05	4.45
30	3.27	2.64
31	3.65	3.56
32	3.93	1.17
33	4.79	2.46
34	5.19	1.52
35	5.85	0.93
36	6.93	-

Reconstructed Path Density

path no.	x-axis (mm)	path density (no. paths/mm)	photon count
41	0.03	0.87	441
42	1.18	11.26	418
43	1.27	22.52	468
44	1.32	19.31	488
45	1.37	22.52	500
46	1.41	27.03	518
47	1.45	27.03	524
48	1.49	27.03	553
49	1.52	33.78	574
50	**1.55**	33.78	574
51	1.58	33.78	574
52	1.61	19.31	571
53	1.67	13.51	550
54	1.74	13.51	526
55	1.81	9.01	491
56	1.92	11.26	435
57	2.01	4.50	376
58	2.23	3.38	288
59	2.53	19.31	259
60	2.58	12.29	259
61	2.66	6.76	271
62	2.81	16.89	309
63	2.87	33.78	329
64	2.90	16.89	300
65	2.96	9.01	335
66	3.07	27.03	341
67	3.11	27.03	350
68	3.15	27.03	300
69	3.18	9.01	332
70	3.22	13.51	365
71	3.29	33.78	347
72	3.34	5.63	379
73	3.52	5.88	312
74	3.69	6.14	282
75	3.85	4.50	250
76	4.07	3.86	182
77	4.33	9.01	147
78	4.44	5.41	147
79	4.63	3.00	141
80	4.96	-	129

.

Weighted average peak locations in the interference patterns in Fig. 2 are given in the following series of tables. Correlations between each set of transverse positions appear in **Fig. 3**, together with peak locations inferred from far-field optics and the equi-distant (path-independent) photon intensity distribution.

Interferogram Intensities (path-based locations)

x-axis (mm)	relative intensity	weight	peak (mm)
	peak -3		
-5.1	0.235	0.131	-0.673
-5.0	0.276	0.154	-0.768
-4.8	0.306	0.171	-0.828
-4.7	0.337	0.189	-0.883
-4.5	0.327	0.183	-0.830
-4.4	0.306	0.171	-0.753
sum:	**1.786**	**1.000**	**-4.734**
	peak -2		
-3.5	0.521	0.140	-0.493
-3.4	0.643	0.173	-0.583
-3.2	0.709	0.191	-0.616
-3.1	0.715	0.193	-0.592
-2.9	0.653	0.176	-0.515
-2.8	0.470	0.127	-0.352
sum:	**3.711**	**1.000**	**-3.151**
	peak -1		
-2.0	0.612	0.132	-0.271
-1.9	0.766	0.166	-0.315
-1.8	0.909	0.196	-0.345
-1.6	0.919	0.199	-0.320
-1.5	0.817	0.177	-0.258
-1.3	0.602	0.130	-0.172
sum:	**4.624**	**1.000**	**-1.681**

x-axis (mm)	relative intensity	weight	peak (mm)
	peak 0		
-0.44	0.561	0.142	-0.062
-0.29	0.827	0.209	-0.061
-0.15	1.000	0.253	-0.037
0.00	0.970	0.245	0.000
0.15	0.602	0.152	0.022
sum:	**3.961**	**1.000**	**-0.138**

x-axis (mm)	relative intensity	weight	peak (mm)
	peak 1		
1.0	0.510	0.093	0.095
1.2	0.664	0.120	0.141
1.3	0.868	0.157	0.207
1.5	0.949	0.172	0.252
1.6	0.960	0.174	0.280
1.8	0.817	0.148	0.260
1.9	0.745	0.135	0.257
sum:	**5.512**	**1.000**	**1.493**
	peak 2		
2.8	0.541	0.117	0.325
2.9	0.592	0.128	0.374
3.1	0.643	0.139	0.426
3.2	0.653	0.141	0.454
3.4	0.633	0.137	0.460
3.5	0.602	0.130	0.456
3.7	0.500	0.108	0.395
3.8	0.470	0.101	0.386
sum:	**4.635**	**1.000**	**3.275**
	peak 3		
4.8	0.265	0.500	2.415
5.0	0.265	0.500	2.488
sum:	**0.531**	**1.000**	**4.902**

Interferogram Intensities (equi-distant locations)

x-axis (mm)	relative intensity	weight	peak (mm)
peak -3			
-4.90	0.008	0.169	-0.827
-4.76	0.009	0.191	-0.911
-4.63	0.010	0.221	-1.023
-4.49	0.010	0.224	-1.006
-4.36	0.009	0.195	-0.850
sum:	**0.046**	**1.000**	**-4.616**
peak -2			
-3.40	0.018	0.160	-0.546
-3.27	0.019	0.176	-0.575
-3.13	0.021	0.187	-0.586
-2.99	0.020	0.183	-0.549
-2.86	0.018	0.163	-0.465
-2.72	0.014	0.131	-0.355
sum:	**0.110**	**1.000**	**-3.076**
peak -1			
-1.91	0.017	0.138	-0.264
-1.77	0.023	0.183	-0.325
-1.63	0.025	0.201	-0.329
-1.50	0.025	0.200	-0.300
-1.36	0.020	0.161	-0.220
-1.23	0.015	0.115	-0.141
sum:	**0.126**	**1.000**	**-1.578**

x-axis (mm)	relative intensity	weight	peak (mm)
peak 0			
-0.41	0.017	0.127	-0.052
-0.27	0.022	0.172	-0.047
-0.14	0.026	0.198	-0.027
0.00	0.026	0.202	0.000
0.14	0.021	0.164	0.022
0.27	0.018	0.137	0.037
sum:	**0.131**	**1.000**	**-0.066**

x-axis (mm)	relative intensity	weight	peak (mm)
peak 3			
4.49			**4.490**
peak 2			
2.59	0.012	0.096	0.247
2.72	0.013	0.107	0.292
2.86	0.014	0.114	0.327
2.99	0.015	0.121	0.362
3.13	0.016	0.126	0.395
3.27	0.015	0.123	0.401
3.40	0.015	0.116	0.393
3.54	0.013	0.103	0.364
3.68	0.012	0.095	0.347
sum:	0.126	1.000	**3.129**
peak 1			
1.23	0.018	0.143	0.175
1.36	0.022	0.175	0.238
1.50	0.025	0.191	0.286
1.63	0.024	0.184	0.300
1.77	0.022	0.171	0.302
1.91	0.018	0.137	0.260
sum:	**0.129**	**1.000**	**1.562**

Reconstructed Paths

x-axis (mm)	relative density	weight	peak (mm)
	peak -3		
-5.1	0.076	0.131	-0.671
-5.1	0.075	0.131	-0.665
-5.0	0.074	0.128	-0.644
-4.9	0.073	0.126	-0.622
-4.9	0.073	0.125	-0.614
-4.9	0.072	0.125	-0.607
-4.7	0.069	0.119	-0.555
-4.5	0.066	0.115	-0.513
sum:	**0.578**	**1.000**	**-4.892**
	peak -2		
-3.5	0.143	0.100	-0.353
-3.4	0.143	0.100	-0.343
-3.3	0.167	0.117	-0.388
-3.2	0.286	0.200	-0.648
-3.2	0.250	0.175	-0.558
-3.1	0.167	0.117	-0.365
-3.0	0.114	0.080	-0.242
-2.9	0.114	0.080	-0.232
-2.8	0.048	0.033	-0.093
sum:	**1.430**	**1.000**	**-3.221**
	peak -1		
-1.9	0.571	0.088	-0.168
-1.8	0.761	0.117	-0.211
-1.7	0.908	0.140	-0.238
-1.6	0.989	0.153	-0.244
-1.5	0.990	0.153	-0.229
-1.4	0.912	0.141	-0.197
-1.3	0.767	0.118	-0.154
-1.2	0.578	0.089	-0.107
sum:	**6.478**	**1.000**	**-1.549**

x-axis (mm)	relative density	weight	peak (mm)
	peak 0		
-0.16	0.286	0.064	-0.010
-0.11	0.182	0.041	-0.005
-0.03	1.000	0.223	-0.007
-0.01	1.000	0.223	-0.003
0.00	1.000	0.223	0.000
0.01	1.000	0.223	0.003
0.03	0.013	0.003	0.000
sum:	**4.480**	**1.000**	**-0.021**

x-axis (mm)	relative density	weight	peak (mm)
	peak 3		
4.3	0.064	0.323	1.399
4.4	0.066	0.331	1.472
4.6	0.068	0.345	1.597
5.0			
sum:	**0.198**	**1.000**	**4.468**
	peak 2		
3.1	0.400	0.174	0.535
3.1	0.400	0.174	0.542
3.1	0.400	0.174	0.548
3.2	0.133	0.058	0.185
3.2	0.200	0.087	0.281
3.3	0.500	0.218	0.718
3.3	0.083	0.036	0.121
3.5	0.087	0.038	0.133
3.7	0.091	0.040	0.146
sum:	**2.295**	**1.000**	**3.209**
	peak 1		
1.2	0.167	0.035	0.041
1.3	0.333	0.069	0.088
1.3	0.286	0.059	0.078
1.4	0.333	0.069	0.095
1.4	0.400	0.083	0.118
1.5	0.400	0.083	0.121
1.5	0.400	0.083	0.124
1.5	0.500	0.104	0.159
1.6	0.500	0.104	0.162
1.6	0.500	0.104	0.165
1.6	0.286	0.059	0.096
1.7	0.200	0.042	0.069
1.7	0.200	0.042	0.072
1.8	0.133	0.028	0.050
1.9	0.167	0.035	0.067
sum:	**4.805**	**1.000**	**1.505**

Bohmian Paths

x-axis (mm)	relative density	weight	peak (mm)
peak -3			
-5.16	0.145	0.518	-2.673
-4.91	0.138	0.482	-2.367
sum:	**0.283**	**1.000**	**-5.040**
peak -2			
-3.51	0.053	0.242	-0.849
-3.24	0.063	0.288	-0.932
-3.02	0.067	0.306	-0.924
-2.81	0.036	0.164	-0.462
sum:	**0.219**	**1.000**	**-3.167**
peak -1			
-1.85	0.059	0.126	-0.232
-1.61	0.333	0.709	-1.141
-1.57	0.059	0.126	-0.197
-1.33	0.019	0.040	-0.054
sum:	**0.470**	**1.000**	**-1.624**

x-axis (mm)	relative density	weight	peak (mm)
peak 0			
-0.11	0.125	0.101	-0.011
0	1.000	0.809	0.000
0.01	0.111	0.090	0.001
sum:	**1.236**	**1.000**	**-0.010**

x-axis (mm)	relative density	weight	peak (mm)
peak 3			
4.79	0.035	1.000	4.790
sum:	**0.035**	**1.000**	**4.790**
peak 2			
3.65	0.050	0.385	1.405
3.27	0.037	0.285	0.932
3.05	0.043	0.330	1.007
sum:	**0.130**	**1.000**	**3.344**
peak 1			
1.85	0.023	0.043	0.013
1.61	0.059	0.110	0.111
1.57	0.333	0.622	0.802
1.29	0.050	0.093	0.146
1.01	0.050	0.093	0.150
0.31	0.020	0.037	0.068
sum:	**0.535**	**0.998**	**1.291**

Far Field Optics

x-axis (mm)	relative intensity	weight	peak (mm)
peak -3			
-5.0	0.564	0.087	-0.435
-4.9	0.755	0.117	-0.571
-4.8	0.904	0.140	-0.670
-4.7	0.987	0.152	-0.717
-4.6	0.992	0.153	-0.704
-4.5	0.916	0.141	-0.637
-4.4	0.773	0.119	-0.525
-4.3	0.586	0.090	-0.389
sum:	**6.477**	**1.000**	**-4.648**
peak -2			
-3.4	0.666	0.112	-0.380
-3.3	0.839	0.141	-0.465
-3.2	0.956	0.161	-0.514
-3.1	1.000	0.168	-0.521
-3.0	0.962	0.162	-0.485
-2.9	0.849	0.143	-0.414
-2.8	0.680	0.114	-0.320
sum:	**5.953**	**1.000**	**-3.099**
peak -1			
-1.9	0.571	0.088	-0.168
-1.8	0.761	0.117	-0.211
-1.7	0.908	0.140	-0.238
-1.6	0.989	0.153	-0.244
-1.5	0.990	0.153	-0.229
-1.4	0.912	0.141	-0.197
-1.3	0.767	0.118	-0.154
-1.2	0.578	0.089	-0.107
sum:	**6.478**	**1.000**	**-1.549**

x-axis (mm)	relative intensity	weight	peak (mm)
peak 0			
-0.30	0.673	0.113	-0.034
-0.20	0.844	0.142	-0.028
-0.10	0.959	0.161	-0.016
0.00	1.000	0.168	0.000
0.10	0.959	0.161	0.016
0.20	0.844	0.142	0.028
0.30	0.673	0.113	0.034
sum:	**5.953**	**1.000**	**0.000**

x-axis (mm)	relative intensity	weight	peak (mm)
peak 3			
4.3	0.586	0.103	0.442
4.5	0.916	0.161	0.723
4.6	0.992	0.174	0.800
4.7	0.987	0.173	0.814
4.8	0.904	0.158	0.761
4.9	0.755	0.132	0.648
5.0	0.564	0.099	0.494
sum:	**5.704**	**1.000**	**4.681**
peak 2			
2.8	0.680	0.114	0.320
2.9	0.849	0.143	0.414
3.0	0.962	0.162	0.485
3.1	1.000	0.168	0.521
3.2	0.956	0.161	0.514
3.3	0.839	0.141	0.465
3.4	0.666	0.112	0.380
sum:	**5.953**	**1.000**	**3.099**
peak 1			
1.2	0.578	0.089	0.107
1.3	0.767	0.118	0.154
1.4	0.912	0.141	0.197
1.5	0.990	0.153	0.229
1.6	0.989	0.153	0.244
1.7	0.908	0.140	0.238
1.8	0.761	0.117	0.211
1.9	0.571	0.088	0.168
sum:	**6.478**	**1.000**	**1.549**

Figure 3 (cont.) Summary of weighted average peak locations in designated distributions.

Peak no.	Interferogram		Recon. paths	Bohmian paths	Far-field optics
	path based	equi-distant			
	x-axis (mm)				
-3	-4.734	-4.616	-4.892	-5.040	-4.684
-2	-3.151	-3.076	-3.221	-3.167	-3.099
-1	-1.681	-1.578	-1.549	-1.624	-1.549
0	-0.138	-0.066	-0.021	-0.010	0
+1	1.493	1.562	1.505	1.291	1.549
+2	3.275	3.129	3.209	3.344	3.099
+3	4.902	4.490	4.468	4.790	4.681